

Note: This is a preprint of a paper being submitted for publication. Contents of this paper should not be quoted nor referred to without permission of the author(s).

7th International Conference on Advanced Nuclear Research  
Takasaki, Japan (March 18-20, 1996)

## New Directions for Ion Beam Processing of Optical Materials

C. W. White, J. D. Budai, J. G. Zhu, and S. P. Withrow  
Oak Ridge National Laboratory  
Oak Ridge, TN

"The submitted manuscript has been authored by a contractor of the U.S. Government under contract No. DE-AC05-96OR22464. Accordingly, the U.S. Government retains a nonexclusive, royalty-free license to publish or reproduce the published form of this contribution, or allow others to do so, for U.S. Government purposes."

Prepared by the  
Oak Ridge National Laboratory  
Oak Ridge, Tennessee 37831  
managed by  
LOCKHEED MARTIN ENERGY RESEARCH CORP.  
for the  
U.S. DEPARTMENT OF ENERGY  
under contract DE-AC05-96OR22464

March 1996

# MASTER

DISTRIBUTION OF THIS DOCUMENT IS UNLIMITED

[Faint, illegible text covering the majority of the page]

## DISCLAIMER

This report was prepared as an account of work sponsored by an agency of the United States Government. Neither the United States Government nor any agency thereof, nor any of their employees, makes any warranty, express or implied, or assumes any legal liability or responsibility for the accuracy, completeness, or usefulness of any information, apparatus, product, or process disclosed, or represents that its use would not infringe privately owned rights. Reference herein to any specific commercial product, process, or service by trade name, trademark, manufacturer, or otherwise does not necessarily constitute or imply its endorsement, recommendation, or favoring by the United States Government or any agency thereof. The views and opinions of authors expressed herein do not necessarily state or reflect those of the United States Government or any agency thereof.



# NEW DIRECTIONS FOR ION BEAM PROCESSING OF OPTICAL MATERIALS

C. W. WHITE, J. D. BUDAI, J. G. ZHU, AND S. P. WITHROW

Oak Ridge National Laboratory  
Oak Ridge, Tennessee 37831-6057

Recent developments in the use of ion implantation to modify the properties of optical materials are summarized. The use of ion implantation to form nanocrystal and quantum dots is emphasized.

Keywords: optical materials, nanocrystals, ion implantation

## 1. Introduction

One of the most promising new directions for ion beam processing of materials involves the use of this technique to modify the properties of optical materials.<sup>1</sup> Historically, the interest in ion beam processing arose through the use of this technique to dope semiconductors. Factors that make this method essential for processing semiconductors are dopant purity (controlled by mass analysis of the ion beam) and profile reproducibility (controlled by the dose and energy). Because of these factors, ion implantation is essential to semiconductor manufacturing today. Ion beam modification has been explored to a much lesser extent as a method to modify the properties of metals and alloys, but already there are numerous examples<sup>2</sup> of the use of this technique to reduce friction, wear, and corrosion, or to change mechanical properties. Ion beam modification of the optical properties of materials by contrast is really in its infancy, and at present it is very much a research tool. However, the technique has already demonstrated some unique features which make it attractive as a method to modify the optical properties of materials. In this paper, we will summarize some of the more recent innovative applications.

## 2. Changes in refractive index

There are a number of mechanisms by which ion beams can be used to modify the properties of optical materials. Damage produced during the implantation process can create stable defects which will absorb or emit light at characteristic wavelengths. Nuclear radiation damage during implantation often leads to a physical decrease in the density of optical material and therefore, to a reduced refractive index. This effect can be used to define optical waveguides. A waveguide is created by having regions of lower refractive index surrounding a region which has a higher index of refraction. The region with higher refractive index can confine light and therefore acts as a waveguide. Waveguides have now been produced in more than 40 optical materials using light ion damage to create regions of lower refractive index.<sup>1</sup> It should also be possible to define buried optical waveguides by this method.

Ion implantation doping has been used also to change the chemical composition of optical materials in order to increase locally the refractive index and thereby to define optical waveguides in the near surface.<sup>3</sup> This has been demonstrated for the case of

Ti implanted at high concentrations into the near surface of LiNbO<sub>3</sub>. During annealing, the implanted Ti becomes substitutional in the lattice and locally increases the refractive index, thus enabling a waveguide to be defined by the implanted region. Figure 1 shows the output intensity pattern of a single-mode ion implanted channel waveguide formed by the implantation of Ti (360 keV,  $2.5 \times 10^{17}/\text{cm}^2$ ) through a mask and into LiNbO<sub>3</sub>, followed by annealing in wet O<sub>2</sub>. The resulting profile of optical intensity measures 1.0  $\mu\text{m}$  deep by  $\sim 1.7 \mu\text{m}$  wide. The width is only about half of the width of the mask ( $\sim 3.5 \mu\text{m}$ ), and this is evidence for a very strong single mode guide which is close to the theoretical limit.

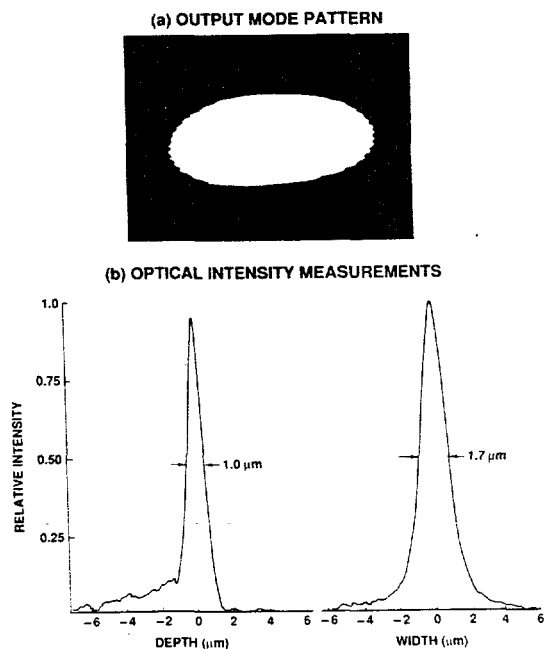


Fig. 1. Channel waveguides fabricated by Ti (360 keV,  $2.5 \times 10^{17}/\text{cm}^2$ ) implantation of LiNbO<sub>3</sub>. The output mode pattern is shown at the top. Intensity measurements in the horizontal and vertical directions are shown on the bottom. The guide was excited by a laser diode ( $\lambda = 0.85 \mu\text{m}$  wavelength) (from ref. 3).

Not only can Ti ion implantation be used to form passive device structures (waveguides) in  $\text{LiNbO}_3$ , it can also be used to fabricate active devices such as modulators because  $\text{LiNbO}_3$  is an electro-optic material. Implantation is particularly attractive for this application because it provides a much higher Ti concentration in a shallower depth than does thermal diffusion. This means that the light can be confined to a smaller volume and for active devices (modulators) this means that less voltage is required for switching. Figure 2 shows schematically a Mach-Zehnder waveguide modulator fabricated by Ti implantation. In this electro-optic device, modulation results from interference produced between phase-coherent light waves that have traveled over different path lengths. The input light splits into two components that travel through the two guides. The effective path length in one of the guides can be varied by the application of a voltage to the electrodes. This results in a phase difference between the two guides that gives rise to interference when the two components are recombined at the output. In Fig. 2, the length of the electrodes is  $\sim 4$  mm and the electrode gap is  $\sim 5$   $\mu\text{m}$ . The output intensity (0.85  $\mu\text{m}$  wavelength) of the modulator as a function of applied voltage is shown. This shows complete modulation with 2.2 V applied, resulting in a VL product of 8.8 V mm and an extinction ratio of  $\sim 14$  dB. This is considerably better than that achieved by thermal diffusion because the size of the mode profile is decreased which allows for higher electric field strengths to be generated by an electrode structure in the area of the greatest optical field confinement. These results demonstrate that ion implantation is potentially a very powerful method for fabricating electro-optic devices in materials such as  $\text{LiNbO}_3$ .

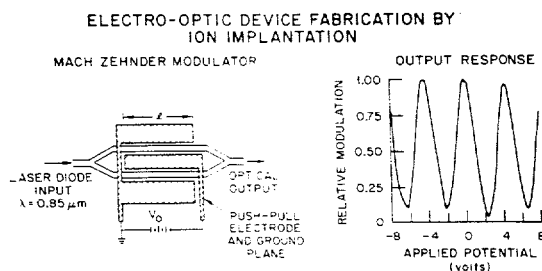


Fig. 2. Mach-Zehnder modulator fabricated by Ti implantation of  $\text{LiNbO}_3$ . The modulator design is illustrated schematically on the left. Output intensity (at 0.85  $\mu\text{m}$ ) as a function of applied voltage is shown on the right (from ref. 3).

### 3. Doping with optically active dopants

Ion implantation doping has also been used to introduce optically active ions into waveguide materials in order to form planar active devices which can be utilized as optical amplifiers and lasers. Doping with rare earth ions such as Er is of tremendous interest because the optical transitions occur at wavelengths near 1.54  $\mu\text{m}$  which is one of

the standard wavelengths used for optical telecommunications. Er has been introduced into a number of optical materials by ion implantation.<sup>4-6</sup> Figure 3 shows the photoluminescence (PL) spectra from Er implanted  $\text{Al}_2\text{O}_3$  excited by 100 mW at 514.5 nm wavelength. PL intensity is increased by a factor of 40 by annealing at 950°C. The inset shows the energy level diagram of the free  $\text{Er}^{3+}$  ion. Using ion implantation,  $\text{Al}_2\text{O}_3$  can be highly doped with optically active Er, making these promising candidates as optical gain media for planar optical amplifiers and lasers.

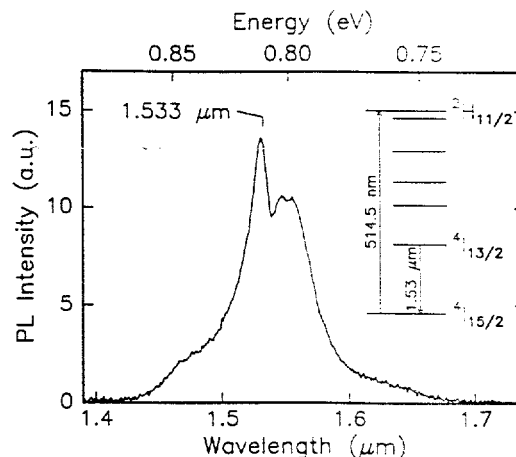


Fig. 3. Room temperature PL spectra from Er (800 keV,  $2.3 \times 10^{15}/\text{cm}^2$ ) implanted  $\text{Al}_2\text{O}_3$  following annealing at 950°C (from ref. 4).

### 4. Formation of nanocrystals and quantum dots

High-dose ion implantation and thermal processing have been used recently in a novel way to form nanocrystals and quantum dots (20–200 Å diameter) in the near-surface region of optical materials.<sup>7</sup> These nanocrystals can produce dramatic changes in the optical properties. Nanocrystals possess unique properties because their surface to volume ratios are enormous, and their energy levels can be shifted considerably due to quantum confinement effects which occur when the dimensions of crystallites are reduced to a size comparable to their excitonic radius. These unique properties have stimulated considerable interest in techniques which can be used to synthesize nanocrystals and control their size and size distribution. Ion implantation is ideally suited to create high densities of nanocrystals in the near-surface region. Implantation is used to create a supersaturated solution in the near surface, and thermal annealing (or implantation at elevated temperatures) leads to precipitation which results in the formation of nanocrystals.

Using the ion implantation method, metallic, elemental semiconductor, and even compound semiconductor nanocrystals can be synthesized in a number of matrices. When produced, they are encapsulated in the matrix, and therefore they do not

have to be packaged subsequently in order to be useful. Ion implantation may be the simplest method to produce some of these nanocrystals due to their sensitivity to oxidizing conditions or high temperatures.

Metallic nanocrystals (Au<sup>9,12-14</sup> or Cu<sup>15,16</sup>) formed in fused silica lead to dramatic changes in the optical properties and give rise to a refractive index which depends on optical intensity. These are, therefore, interesting candidates as nonlinear optical materials. Elemental semiconductor nanocrystals can be formed by the implantation of Si or Ge, and these elemental semiconductor nanocrystals can exhibit strong PL in the visible and near IR regions.<sup>11,17-21</sup> In crystalline  $\alpha$ -Al<sub>2</sub>O<sub>3</sub>, nanocrystals of Si or Ge can be produced by implantation, and these are three dimensionally oriented with respect to the lattice.<sup>22</sup> Finally, compound semiconductor nanocrystals have been produced in SiO<sub>2</sub> and Al<sub>2</sub>O<sub>3</sub> by implanting various combinations of ions.<sup>7,8,10,25</sup> Compound semiconductor nanocrystals are expected to exhibit strong optical nonlinearities and a fast response time.<sup>23</sup>

In the work to be described, ions were implanted into fused silica (Corning 7940), thermally oxidized silicon wafers, or  $\alpha$ -Al<sub>2</sub>O<sub>3</sub>(0001) to doses of  $\sim 1 \times 10^{17}/\text{cm}^2$  at energies chosen to give a projected range of  $\sim 100$  nm or greater. To form compounds or alloys, various combinations of ions were implanted at energies chosen to give an overlap of the profiles. Implanted samples were annealed in flowing Ar + 4% H<sub>2</sub> to induce precipitation and compound formation. Characterization methods include x-ray diffraction, Rutherford backscattering ion channeling (2.3 MeV He ions), cross-section transmission electron microscopy (TEM), Raman spectroscopy, and various types of optical measurements (absorption, PL, and infrared reflectivity).

Figure 4 shows the high density of Au nanocrystals formed in fused silica by the

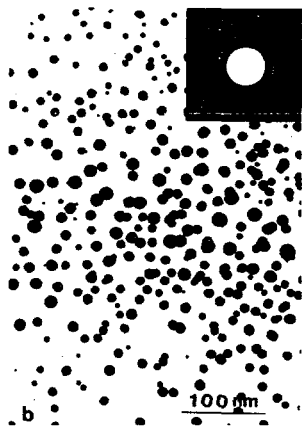


Fig. 4. Cross-section TEM micrograph showing Au nanocrystals formed in fused silica by Au (2.75 MeV,  $1.5 \times 10^{17}/\text{cm}^2$ ) implantation at 600°C.

implantation of Au at elevated temperatures.<sup>9</sup> Individual nanocrystals are spherical and oriented at random relative to each other. Following implantation, the implanted region is deep red in color. The presence of these nanocrystals gives rise to strong optical absorption at the surface plasmon resonance energy, as shown by the intense optical absorption band at  $\sim 2.35$  eV in Fig. 5. If implantation is done at room temperature, the mobility of the Au is too low for nanocrystals to form, and the optical absorption does not exhibit the strong absorption band at the surface plasmon resonance energy. The size and size distribution of nanocrystals are strongly dependent on the implantation/annealing conditions as shown in Fig. 6. The average size can be varied from  $\sim 25$  Å to  $\sim 125$  Å by changes in the implantation or annealing conditions.

The presence of these nanocrystals at high concentrations in the near surface gives rise to a refractive index which is strongly dependent on the light intensity:

$$n = n_0 + n_2 I \quad (1)$$

where  $n_0$  is the intensity independent index,  $n_2$  is the intensity dependent term and  $I$  is the light intensity. For Au nanocrystals in fused silica, the value for  $n_2$  is of the order of  $10^{-9}\text{cm}^2/\text{watt}$  at a wavelength of 570 nm and a volume fraction of  $\sim 10\%$ <sup>9,12,14</sup> and values for  $n_2$  scale linearly with ion dose or volume fraction. These large values of  $n_2$  and a response time in the picosecond regime<sup>24</sup> make these interesting candidates as nonlinear optical materials.

Si and Ge nanocrystals can be synthesized in both SiO<sub>2</sub><sup>11,17-21</sup> and Al<sub>2</sub>O<sub>3</sub><sup>22</sup> by ion implantation. Figure 7 shows a high resolution

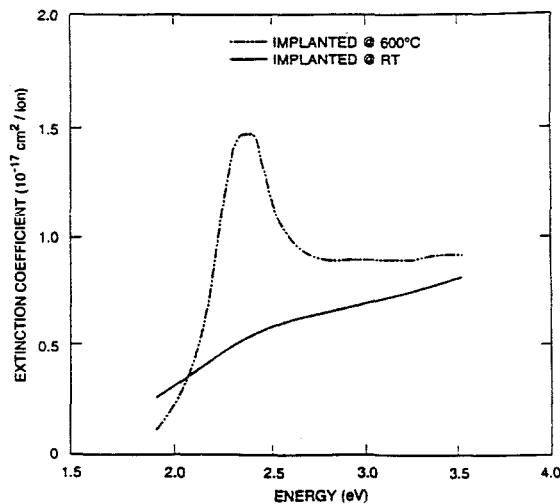


Fig. 5. Optical absorption for fused silica samples implanted by Au (2.75 MeV,  $1.5 \times 10^{17}/\text{cm}^2$ ) at 600°C and at room temperature.

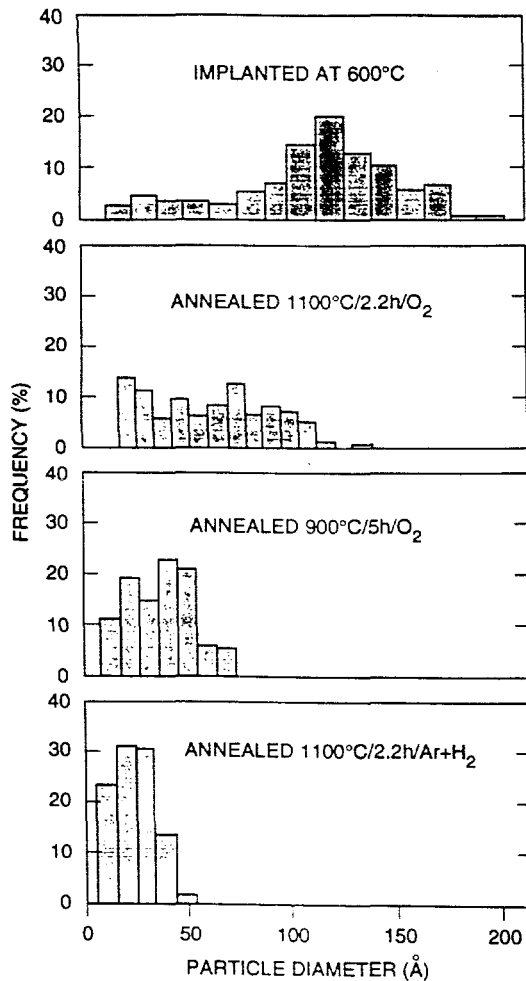


Fig. 6. Size distribution for Au nanocrystals in fused silica. Samples were implanted by Au (2.75 MeV,  $1.5 \times 10^{17}/\text{cm}^2$ ). The top distribution was measured following implantation at 600°C. The other three were measured after annealing samples implanted at room temperature.

micrograph for silicon nanocrystals in SiO<sub>2</sub> formed by Si implantation. Under these conditions, the average nanocrystal diameter is ~4 nm and there are very few nanocrystals larger than 8 nm in diameter. The presence of these small Si nanocrystals in the near-surface region give rise to strong PL in the near IR region. Figure 8 compares PL spectra from implanted samples in the as-implanted state and after annealing. In the as-implanted state, the PL spectra shows a band peaked at ~640 nm which arises from defects introduced into SiO<sub>2</sub> during implantation. Annealing at 1100°C results in the formation of Si nanocrystals and the PL intensity from Si implanted SiO<sub>2</sub> is comparable to that from porous Si but shifted in wavelength, as demonstrated by the results in Fig. 9. The large intensities of PL from Si implanted SiO<sub>2</sub> and its greater stability compared to radiation from porous Si make the implanted

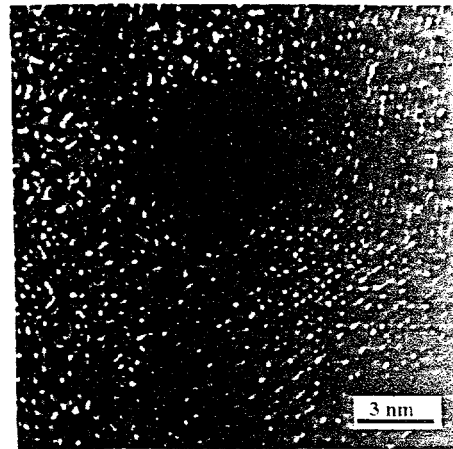


Fig. 7. High-resolution, cross-section micrograph showing Si nanocrystals formed by Si (400 keV,  $6 \times 10^{17}/\text{cm}^2$ , RT) implantation of SiO<sub>2</sub>, followed by thermal annealing (1100°C/1 h).

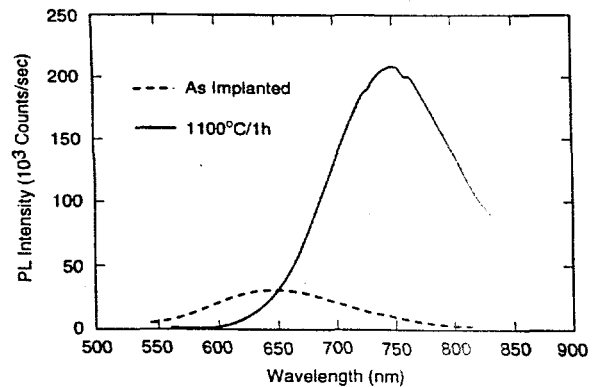


Fig. 8. PL arising from SiO<sub>2</sub> implanted by Si (400 keV,  $6 \times 10^{17}/\text{cm}^2$ ) in the as-implanted state and after annealing at 1100°C/1 h.

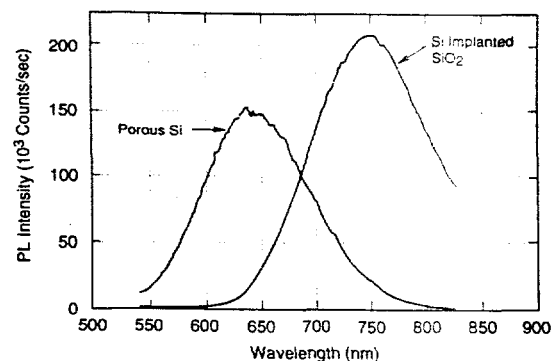


Fig. 9. PL arising from porous Si and from Si (400 keV,  $6 \times 10^{17}/\text{cm}^2$ ) implanted SiO<sub>2</sub> following annealing at 1100°C/1 h.

nanocomposites interesting candidates as display materials. The peak in the PL spectra can be shifted to higher photon energies by reducing the implantation dose (and therefore reducing the particle size). This is consistent with the behavior expected if the radiation arises from quantum confined excitons, but interface states at the nanocrystal/oxide interface may be the states giving rise to the PL radiation.

Compound semiconductor nanocrystals have even been formed by ion implantation.<sup>7,8,10,25</sup> In all previous experiments on compound formation during implantation, the matrix material was one of the major components of the compound. Recently, it has been demonstrated that compounds and alloys can be formed by sequential implantation of both constituents at energies chosen to give an overlap of the profiles, followed by annealing. Figure 10 shows x-ray diffraction results demonstrating that GaAs can be formed in SiO<sub>2</sub> by ion implantation.<sup>8,10</sup> Equal doses ( $1.5 \times 10^{17}/\text{cm}^2$ ) of Ga and As were implanted into SiO<sub>2</sub>. Following annealing (1000°C/1 h), the x-ray diffraction results show several lines arising from zincblende GaAs in addition to the expected scattering from SiO<sub>2</sub>. TEM measurements show that GaAs nanocrystals up to several hundred Angstroms in diameter can be formed, and the size and size distribution depend strongly on the dose, annealing conditions, and the order of the implant.<sup>25</sup>

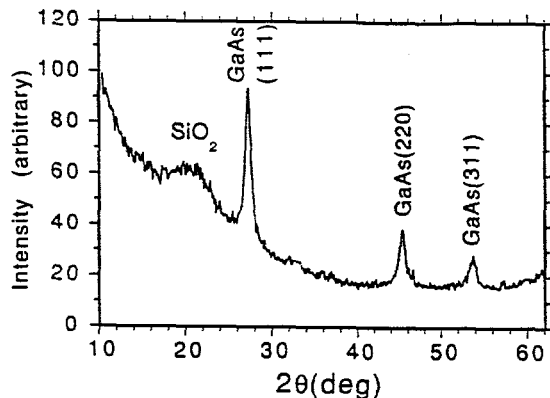


Fig. 10. X-ray diffraction results showing GaAs nanocrystals formed by sequential implantation of Ga and As into SiO<sub>2</sub> followed by annealing.

GaAs nanocrystals can even be formed in Al<sub>2</sub>O<sub>3</sub> by sequential ion implantation.<sup>10</sup> Figure 11 shows x-ray diffraction  $\theta$ - $2\theta$  scans along the *c*-axis of Al<sub>2</sub>O<sub>3</sub> after implantation of equal doses ( $1 \times 10^{17}/\text{cm}^2$ ) of Ga and As followed by thermal annealing (1100°C/1 h). The intense (0006) reflection from Al<sub>2</sub>O<sub>3</sub> (at  $2\theta \approx 41.7^\circ$ ) is observed along with a number of peaks identified as arising from zincblende GaAs. By far, the strongest of these peaks is that arising from GaAs (111). This demonstrates that the GaAs nanoparticles have a tendency to orient with their (111) planes parallel to the *c* planes of Al<sub>2</sub>O<sub>3</sub>. Not only are the nanoparticles oriented with respect to

the surface normal, they also exhibit strong in-plane alignment, and therefore the GaAs nanoparticles formed by sequential ion implantation are three dimensionally oriented in Al<sub>2</sub>O<sub>3</sub>.

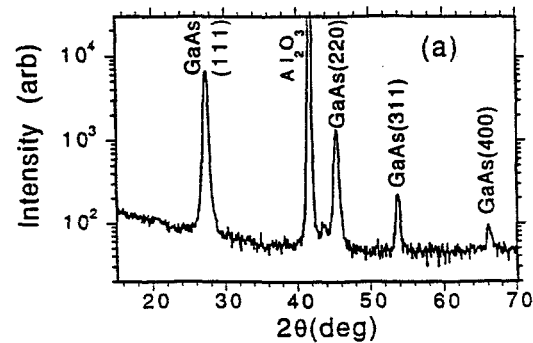


Fig. 11. X-ray diffraction from GaAs nanocrystals in Al<sub>2</sub>O<sub>3</sub>.

GaAs nanocrystals have even been synthesized in crystalline Si by sequential ion implantation.<sup>26</sup> This is demonstrated by the x-ray diffraction results of Fig. 12 which shows  $\theta$ - $2\theta$  scans along the [001] direction. This shows the expected Si(004) reflection along with strong peaks identified as arising from GaAs. Similar to the case of Al<sub>2</sub>O<sub>3</sub>, we find that GaAs nanoparticles in Si are three dimensionally oriented with the matrix.

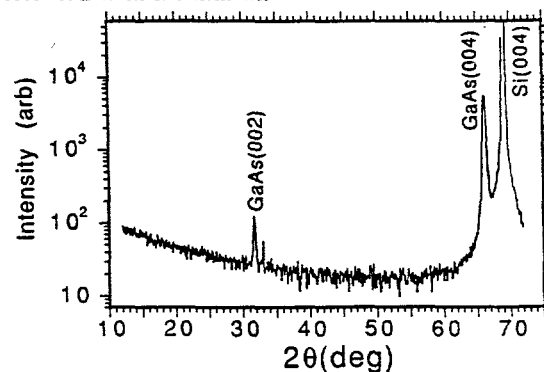


Fig. 12. X-ray diffraction from GaAs nanocrystals embedded in Si by sequential ion implantation.

The synthesis of compounds by sequential ion implantation represents a new direction of research for high-dose ion implantation. It greatly extends the potential applications of ion beam synthesis because it presents opportunities to form many more compounds and alloys than previously demonstrated. These compounds can be synthesized in a variety of matrices. Table 1 provides a list of compound semiconductor nanocrystals which we have produced in SiO<sub>2</sub>, Al<sub>2</sub>O<sub>3</sub>, and single-crystal Si. In most cases, positive identification of the compound was obtained from diffraction measurements. Results shown in this table demonstrate the wide range of compounds and alloys which can be formed. The synthesis of compounds by sequential implantation

should find extensive applications in these and other matrices.

Table 1. Nanocrystal compounds formed by sequential implantation. An x indicates that the compound was formed in the given matrix.

Nanocrystal	Substrate		
	SiO <sub>2</sub>	Al <sub>2</sub> O <sub>3</sub>	Si
SiGe	x	x	
GaAs	x	x	x
InAs	x		
GaP	x		x
InP	x		
CdS	x	x	x
CdSe	x	x	
CdSe <sub>0.5</sub> S <sub>0.5</sub>	x		
GaN		x	

#### Acknowledgment

Oak Ridge National Laboratory, managed by Lockheed Martin Energy Research Corp. for the U.S. Department of Energy under contract number DE-AC05-96OR22464.

#### References

1. P. D. Townsend, P. J. Chandler, and L. Zhang, *Optical Effects of Ion Implantation* (Cambridge University Press, Cambridge, Great Britain) 1994.
2. See numerous examples in the proceedings of the recent International Conference on Ion Beam Modification of Materials: *Nucl. Inst. and Methods B* 106 (1996); *Nucl. Inst. and Methods B* 80/81 (1993); *Nucl. Inst. and Methods B* 59/60 (1991); *Nucl. Inst. and Methods B* 39 (1989).
3. P. R. Ashley, W. S. C. Chang, C. J. Buchal, and D. K. Thomas, *J. Lightwave Technology* 7, 855 (1989).
4. G. N. van den Hoven, E. Snoeks, A. Polman, J. W. M. van Uftelen, Y. S. Oei, and M. K. Smit, *Appl. Phys. Letts.* 62, 3065 (1993).
5. A. Polman, D. C. Jacobson, D. J. Eaglesham, R. C. Kistler, and J. M. Poate, *J. Appl. Phys.* 70, 3778 (1991).
6. E. Snoeks, G. N. van den Hoven, and A. Pollman, *J. Appl. Phys.* 73, 8179 (1993).
7. C. W. White, J. D. Budai, J. G. Zhu, S. P. Withrow, D. M. Hembree, D. O. Henderson, A. Ueda, Y. S. Tung, and R. Mu, *Mat. Res. Soc. Symp. Proc.* 396, 377 (1996).
8. C. W. White, J. D. Budai, J. G. Zhu, S. P. Withrow, R. A. Zuhr, Y. Chen, D. M. Hembree, R. H. Magruder, and D. O. Henderson, *Mat. Res. Soc. Symp. Proc.* 358, 169 (1995).
9. C. W. White, D. S. Zhou, J. D. Budai, R. A. Zuhr, R. H. Magruder, and D. H. Osborne, *Mat. Res. Soc. Symp. Proc.* 316, 499 (1994).
10. C. W. White, J. D. Budai, J. G. Zhu, S. P. Withrow, R. A. Zuhr, D. M. Hembree, D. O. Henderson, A. Ueda, Y. S. Tung, R. Mu, and R. H. Magruder, *J. Appl. Phys.* 79, 1876 (1996).
11. J. G. Zhu, C. W. White, J. D. Budai, S. P. Withrow, and Y. Chen, *J. Appl. Phys.* 77, 4386 (1995).

12. R. H. Magruder, L. Yang, R. F. Haglund, C. W. White, C. Yang, R. Dorsinville, and R. R. Alfando, *Appl. Phys. Lett.* 62, 1730 (1993).
13. G. W. Arnold, *J. Appl. Phys.* 46, 4466 (1975).
14. K. Fukuami, A. Chayahara, M. Satou, J. Hayakawa, M. Hangyo, S. Nakashima, *Jap. J. Appl. Phys.* 30, L742 (1991).
15. R. H. Magruder, R. F. Haglund, L. Yang, J. E. Wittig, and R. A. Zuhr, *J. Appl. Phys.* 76, 708 (1994).
16. R. F. Haglund, L. Yang, R. H. Magruder, J. E. Wittig, K. Becker, and R. A. Zuhr, *Opt. Lett.* 18, 373 (1993).
17. H. Atwater, K. V. Shcheglov, S. S. Wong, K. J. Vahala, R. C. Flagan, M. L. Brongersma, and A. Polman, *Mat. Res. Soc. Symp. Proc.* 316, 409 (1994).
18. H. Takagi, H. Ogawa, Y. Yamazaki, A. Ishizaki, and T. Nakagiri, *Appl. Phys. Lett.* 56, 2379 (1990).
19. Y. Maeda, N. Tsukamoto, Y. Yazawa, Y. Kanemitsu, and Y. Masumoto, *Appl. Phys. Lett.* 59, 3168 (1991).
20. T. Shimizu-Iwayama, K. Fujita, S. Nakao, K. Saitoh, T. Fujita, and N. Itoh, *J. Appl. Phys.* 75, 7779 (1994).
21. J. G. Zhu, C. W. White, J. D. Budai, S. P. Withrow, and Y. Chen, *Mat. Res. Soc. Symp. Proc.* 358, 175 (1995).
22. C. W. White, J. D. Budai, S. P. Withrow, S. J. Pennycook, D. M. Hembree, Jr., D. S. Zhou, T. Yo-Dihn, and R. H. Magruder, *Mat. Res. Soc. Symp. Proc.* 316, 487 (1994).
23. R. K. Jain and R. C. Lind, *J. Opt. Soc. Am.* 73, 647 (1983).
24. F. Hache, D. Ricard, C. Flyzannis, and U. Kreibig, *Appl. Phys.* A47, 347 (1988).
25. J. G. Zhu, C. W. White, D. J. Wallis, J. D. Budai, S. P. Withrow, and D. O. Henderson, *Mat. Res. Soc. Symp. Proc.* 396 (1996), in press.
26. C. W. White, J. D. Budai, J. G. Zhu, S. P. Withrow, and M. J. Aziz, *Applied Physics Letters* (in press).